CHAPTER V

Combined Effects of Hall and Ion-Slip Currents on Steady Free-Convective Flow of an Incompressible Viscous and Electrically Conducting Fluid with Heat and Mass Transfer over a Porous Flat Plate Embedded in Porous Medium

5.1. Introduction

A few decades ago, many researchers paid more attention to MHD fluid flow problems but ignored the Hall current and ion-slip current in Ohms law. The MHD heat and mass transfer flow under the strong magnetic field plays a key role in many engineering problems such as astrophysics, chemical engineering and geophysics. In flows of laboratory plasma, Hall and ion-slip currents are likely to be important. Hence it is now proposed to study heat and mass transfer of a free convection MHD flow past an infinite vertical porous plate taking into account Hall and ion-slip currents.

Combined effects of Hall and ion-slip currents on free convective flow past a semi-infinite vertical plate was investigated by Abo-Eldahab and Aziz (2000). The effect of Hall and ion-slip currents on fully developed electrically conducting fluid flow between vertical parallel plates in the presence of a temperature dependent heat source was investigated using homotopy analysis method by Srinivasacharya and Kaladhar (2012). Later, Darbhasayanam Srinivasacharya and Kolla Kaladhar (2012) considered the effect of Hall and ion-slip currents on electrically conducting couple stress fluid flow between two circular cylinders in the presence of a temperature dependent heat source. Steady motion of electrically conducting viscous fluid in the presence of Hall current was studied by Tani (1962).

The effects of Hall, ion-slip currents and variable thermal diffusivity on magnetomicropolar fluid flow, heat and mass transfer with suction through a porous medium was numerically analyzed by Motsa and Shateyi (2012). Attia (2002) studied the flow of a dusty fluid in the presence of Hall and ion slip current using analytical procedure. Shampa Ghosh (2015) studied magneto hydrodynamic boundary layer flow over a stretching sheet with chemical reaction.

The heat transfer of MHD Couette flow in the presence of Hall and ion-slip currents was studied by Soundelgekar *et al.* (1979). Unsteady MHD Couette flow of

an incompressible viscous fluid in the presence of Hall and ion-slip currents in a porous medium was studied by Nirmal Ghara *et al.* (2012). The unsteady Couette flow of an electrically conducting viscous incompressible fluid between two parallel horizontal non-conducting porous plates with heat transfer in the presence of ion-slip was studied by Attia (2005).

The absence of Hall current and ion-slip current in Shampa Ghosh (2015) motivated us to take up the present work wherein we study the effect of Hall current and ion-slip current on heat and mass transfer in a steady free-convective flow in the presence of a uniform transverse magnetic field in a porous medium. The governing equations are transformed by a similarity transformation into a system of non-linear ordinary differential equations which are solved numerically by fourth order Runge-Kutta Method. Numerical calculations are performed for various values of the magnetic parameter, Hall current parameter, Ion-slip parameter, Schimdt number and Soret number. The results are given for the coefficients of skin-friction, rate of heat transfer and rate of mass transfer for various values of magnetic, Hall current and Ion-slip parameters.

5.2. Flow Description and Governing Equations

We consider a steady free-convective laminar flow of an incompressible viscous and electrically conducting fluid with heat and mass transfer over a porous flat plate in the presence of transverse magnetic field. Magnetic field is assumed to be strong enough to produce Hall and ion-slip currents. We choose a stationary frame of reference (x, y, z) such that x-axis is chosen along the direction of motion, y-axis is normal to the surface and z-axis is transverse to the xy-plane. For an electrically conducting fluid, the Hall and ion-slip currents affect the flow significantly in the presence of large magnetic field. The temperature and the concentration profiles are maintained at prescribed constant values T_w, C_w at the plate and T_∞, C_∞ are the fixed values far away from the sheet.

In the present work, the following assumptions are made:

- Flow of a Newtonian and electrically conducting fluid is considered which is steady, viscous, incompressible and laminar in nature.
- The fluid is flowing over a horizontal plate in the x-direction.
- A strong transverse magnetic field $\vec{B}_0$ with constant intensity is present along the y-axis.

- The Hall and ion slip effects are considered in the flow.
- An electrically conducting fluid is affected by Hall and ion-slip currents in the presence of magnetic field.
- Body forces in the momentum equation are neglected.
- Heat source is assumed to be absent.
- Thermo diffusion effects are considered.

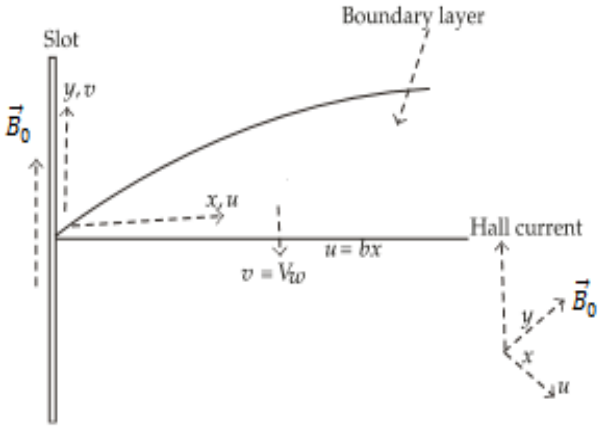

Fig 5.1 Schematic diagram of the problem

Owing to the above assumptions, the free-convection flow with heat and mass transfer and generalized Ohm's law with Hall current effect are governed by the following system of equations:

$$\frac{\partial u}{\partial x}+\frac{\partial v}{\partial y}=0 \tag{5.1}$$

$$u\frac{\partial u}{\partial x}+v\frac{\partial u}{\partial y}=\gamma\frac{\partial^2 u}{\partial y^2}-\frac{\gamma}{k}u-\frac{B_0}{\rho}j_z \tag{5.2}$$

$$u\frac{\partial w}{\partial x}+v\frac{\partial w}{\partial y}=\gamma\frac{\partial^2 w}{\partial y^2}-\frac{\gamma}{k}w+\frac{B_0}{\rho}j_x \tag{5.3}$$

$$u\frac{\partial T}{\partial x}+v\frac{\partial T}{\partial y}=\frac{\kappa}{\rho C_p}\frac{\partial^2 T}{\partial y^2} \tag{5.4}$$

$$u\frac{\partial C}{\partial x}+v\frac{\partial C}{\partial y}=D_M\frac{\partial^2 C}{\partial y^2}+D_T\frac{\partial^2 T}{\partial y^2} \tag{5.5}$$

In the above system of equations, (u,v,w) are the velocity components along the (x,y,z) directions respectively. $T, C, \rho, \sigma,\ U_\infty$ and $\gamma=(\mu/\rho)$ represent respectively the temperature, mass concentration, coefficient of viscosity, density, constant electrical conductivity, free stream velocity and kinematic viscosity of the fluid. The constant parameters in the system: $k, C_p, \kappa,\ D_M$ and D_T represent respectively the permeability of porous material, specific heat at constant pressure,

thermal conductivity of the fluid, molecular diffusivity and thermal diffusivity. $\vec{B}(x)$ is the magnetic field in the y-direction and is given by $\vec{B}(x) = B_0/(x)^{1/2}$.

The equation of conservation of electric charge $\nabla.\vec{J} = 0$ gives j_y= constant, where $\vec{J} = (j_x, j_y, j_z)$. This constant is assumed to be zero, since $j_y = 0$ everywhere in the flow. The current density components j_x and j_z are obtained from the generalized Ohm's law in the following form,

$$\vec{J} = \frac{\sigma}{1+m^2}\left(\vec{E} + \vec{V} \times \vec{B} - \frac{1}{en_e}\vec{J} \times \vec{B}\right)$$

in which $\vec{V}, \vec{E}, \vec{B}, \vec{J}, m = \frac{\sigma B_0}{en_e}, \sigma, e$ and n_e represent the velocity vector, intensity vector of the electric field, magnetic vector, electric current density vector, Hall parameter, electrical conductivity, charge of the electron and number density of the electron. The current density components are given by,

$$j_x = \frac{\sigma}{\alpha_e^2 + \beta_e^2}[\alpha_e(E_x - wB_0) + \beta_e(E_z + uB_0)]$$

$$j_z = \frac{\sigma}{\alpha_e^2 + \beta_e^2}[\alpha_e(E_z + uB_0) - \beta_e(E_x - wB_0)]$$

where β_e is the Hall current parameter, β_i is the Ion-slip parameter and $\alpha_e = 1 + \beta_i\beta_e$. In the absence of electric field ($E_x = E_z = 0$), we get

$$j_x = \frac{\sigma B_0}{\alpha_e^2 + \beta_e^2}[\beta_e u - \alpha_e w]$$

$$j_z = \frac{\sigma B_0}{\alpha_e^2 + \beta_e^2}[\alpha_e u + \beta_e w]$$

The governing equations (5.1)-(5.5) become,

$$\frac{\partial u}{\partial x} + \frac{\partial v}{\partial y} = 0 \qquad (5.6)$$

$$u\frac{\partial u}{\partial x} + v\frac{\partial u}{\partial y} = \gamma\frac{\partial^2 u}{\partial y^2} - \frac{\gamma}{k}u - \frac{\sigma B_0^2}{\rho(\alpha_e^2+\beta_e^2)}(\alpha_e u + \beta_e w) \qquad (5.7)$$

$$u\frac{\partial w}{\partial x} + v\frac{\partial w}{\partial y} = \gamma\frac{\partial^2 w}{\partial y^2} - \frac{\gamma}{k}w + \frac{\sigma B_0^2}{\rho(\alpha_e^2+\beta_e^2)}(\beta_e u - \alpha_e w) \qquad (5.8)$$

$$u\frac{\partial T}{\partial x} + v\frac{\partial T}{\partial y} = \frac{\kappa}{\rho C_p}\frac{\partial^2 T}{\partial y^2} \qquad (5.9)$$

$$u\frac{\partial C}{\partial x} + v\frac{\partial C}{\partial y} = D_M\frac{\partial^2 C}{\partial y^2} + D_T\frac{\partial^2 T}{\partial y^2} \qquad (5.10)$$

The appropriate boundary conditions for the velocity, temperature and mass concentration are given by,

$u = bx, v = -V_w$, $w = 0$ at y=0; $u = w = 0$ as $y \to \infty$, (5.11)

$T = T_w$ at $y = 0$; $T \to T_\infty$ as $y \to \infty$, (5.12)

$C = C_w$ at $y = 0$; $C \to C_\infty$ as $y \to \infty$, (5.13)

where b>0 being stretching rate of the sheet, V_w is suction/injection velocity.

5.3. Solution of the Problem

We use similarity technique to solve the system of equations (5.6)-(5.10) along with the boundary conditions (5.11)-(5.13). The similarity transformations are,

$$u = bxf'(\eta),\ v = -\sqrt{b\gamma}f(\eta),\ w = \sqrt{b\gamma}g(\eta),\ \eta = \sqrt{\frac{b}{\gamma}}\,y,\ \theta(\eta) = \frac{T-T_\infty}{T_w-T_\infty},$$

$$\phi(\eta) = \frac{C-C_\infty}{(C_w-C_\infty)} \quad (5.14)$$

Introducing the above transformations in equations (5.6)-(5.10) we obtain the following system of ordinary differential equations,

$$f''' + ff'' - f'^2 - \frac{M}{(\alpha_e^2+\beta_e^2)}(\alpha_e f' + \frac{\beta_e}{\sqrt{Re}}g) - \frac{1}{k^*}f' = 0, \quad (5.15)$$

$$g'' + fg' + \frac{M}{(\alpha_e^2+\beta_e^2)}(\beta_e\sqrt{Re}f' - \alpha_e g) - \frac{1}{k^*}g = 0, \quad (5.16)$$

$$\theta'' + Prf\theta' = 0, \quad (5.17)$$

$$\phi'' + Scf\phi' + ScSr\theta'' = 0. \quad (5.18)$$

where $M = \frac{\sigma B_0^2}{\rho b}$ is the magnetic parameter, $Pr = \mu C_p/\kappa$ is the Prandtl number, $Sc = \frac{\gamma}{D_m}$ is the Schmidt number, $Sr = \frac{(T_w-T_\infty)D_T}{(C_w-C_\infty)\gamma}$ is the Soret number, $k^* = kb/\gamma$ is the permeability of porous medium and $Re_x = \frac{bx^2}{\gamma}$ is the Reynolds number.

In view of the similarity transformations, the boundary conditions (5.11)-(5.13) transform to the following form,

$f(\eta) = S$, $f'(\eta) = 1$ at $\eta = 0$; $f'(\eta) \to 0$ as $\eta \to \infty$ (5.19)

$g(\eta) = 0$ at $\eta = 0$; $g(\eta) \to 0$ as $\eta \to \infty$ (5.20)

$\theta(\eta) = 1$ at $\eta = 0$; $\theta(\eta) \to 0$ as $\eta \to \infty$ (5.21)

$\phi(\eta) = 1$ at $\eta = 0$; $\phi(\eta) \to 0$ as $\eta \to \infty$ (5.22)

where $S = V_w/\sqrt{b\gamma}$ is the mass transfer coefficient such that $S > 0$ indicates suction, $S < 0$ indicates blowing at the surface.

The non-linear coupled ordinary differential equations (5.15)-(5.18) subject to boundary conditions (5.19)-(5.22) are solved numerically using fourth order Runge-Kutta method.

$f' = w$, $w' = v$, $\theta = y$, $\theta' = z$, $\phi = b$, $\phi' = e$, $g = i$, $g' = a$.

$$v' = -fv + w^2 + \frac{M}{(\alpha_e^2+\beta_e^2)}\left(\alpha_e w + \frac{\beta_e}{\sqrt{Re}} i\right) + \frac{1}{k^*} w, \quad (5.23)$$

$$a' = -fa - \frac{M}{(\alpha_e^2+\beta_e^2)}\left(\beta_e \sqrt{Re} w - \alpha_e i\right) + \frac{1}{k^*} i \quad (5.24)$$

$$z' = -Prfz, \quad (5.25)$$

$$e' = -Scfe - ScSrz' \quad (5.26)$$

and boundary conditions become,

$$f(0) = S,\ w(0) = 1,\ i(0) = 0,\ \ y(0) = 1,\ \ b(0) = 1 \ \text{ at } \eta = 0 \quad (5.27)$$

$$w(0) \to 0, a(0) \to 0, y(0) \to 0,\ b(0) \to 0 \text{ as } \eta \to \infty \quad (5.28)$$

The above system of ODEs is reduced to a system of first order differential equations which is solved by shooting procedure using fourth order Runge Kutta method.

The major physical quantities of engineering interest the skin-friction coefficient C_f , the local Nusselt number Nu_x, and the local Sherwood number Sh_x are defined respectively as follows,

Skin-friction co-efficient:

$C_{fx} = \frac{\tau_x}{\mu bx\sqrt{\frac{b}{\gamma}}}$, Here Shear stress along x-direction

$C_{fz} = \frac{\tau_z}{\mu\sqrt{b\gamma}\sqrt{\frac{b}{\gamma}}}$, Here Shear stress along z-direction (5.29)

Local Nusselt number: $Nu_x = \frac{q_w}{k\sqrt{\frac{b}{\gamma}}(T_w - T_\infty)}$ (5.30)

Local Sherwood number: $Sh_x = \frac{m_w}{D\sqrt{\frac{b}{\gamma}}(C_w - C_\infty)}$ (5.31)

where τ_x and τ_z represent skin-friction along x and z- direction respectively, q_w is the heat flux, and m_w is the mass flux at the surface.

$$\tau_x = \mu\left(\frac{\partial u}{\partial y}\right)_{y=0} = \mu bx\sqrt{\frac{b}{\gamma}} f''(0)\ ;\ \tau_z = \mu\left(\frac{\partial w}{\partial y}\right)_{y=0} = \mu\sqrt{b\nu}\sqrt{\frac{b}{\gamma}} g'(0) \quad (5.32)$$

$$q_w = -k\left(\frac{\partial T}{\partial y}\right)_{y=0} = -k\sqrt{\frac{b}{\gamma}}\,(T_w - T_\infty)\theta'(0) \quad (5.33)$$

$$m_w = -D\left(\frac{\partial C}{\partial y}\right)_{y=0} = -D\sqrt{\frac{b}{\gamma}}\,(C_w - C_\infty)\phi'(0) \quad (5.34)$$

Substituting equations (5.32), (5.33) and (5.34) into the equations (5.29), (5.30) and (5.31) we get

$$f''(0) = C_{fx}$$

$$g'(0) = C_{fz}$$

$$-\theta'(0) = Nu_x$$
$$-\phi'(0) = Sh_x$$

5.4. Results and Discussion

The numerical computations are performed for several values of dimensionless parameters involved in the equations i.e., magnetic parameter M, Hall current β_e, Ion-slip parameter β_i, Schmidt number Sc, Soret number Sr, Suction/Blowing parameter S. In order to examine the computed results and understand the bahaviour of various physical parameters of the flow, numerical values for the distributions of velocity, temperature, concentration, skin friction, Nusselt number and Sherwood number are calculated by fixing various values for the non dimensional parameters of physical interest.

Figures (5.2)-(5.4) show the effect of Hall current parameter β_e on the velocity components $f'(\eta)$, $f(\eta)$ and $g(\eta)$. It can be observed from figures (5.2)-(5.3) that axial velocity $f'(\eta)$ and transverse velocity $f(\eta)$ increase as Hall current parameter β_e increases. Figure (5.4) depicts that cross flow velocity $g(\eta)$ increases with increasing values of β_e when $\beta_e \leq 1$, but decreases with increasing values of Hall current parameter β_e greater than unity. Figure (5.5) shows the effect of Hall current parameter β_e on concentration profile $\phi(\eta)$. From this, we observe that the concentration decreases with increasing values of β_e .

Figures (5.6)-(5.8) show the influence of magnetic parameter on the velocity components $f'(\eta)$, $f(\eta)$ and $g(\eta)$. From figures (5.6)-(5.7) we observe that the axial and transverse velocities decrease with the increase of the magnetic field parameter values whereas the cross flow velocity $g(\eta)$ increases with increasing values of M.

Figures (5.9)-(5.11) show the effect of ion-slip parameter β_i on the velocity components $f'(\eta)$, $f(\eta)$ and $g(\eta)$. It is found that axial velocity $f'(\eta)$ and transverse velocity of $f(\eta)$ increase as β_i increases and cross flow velocity $g(\eta)$ decreases with increasing values of β_i.

From figures (5.12)-(5.13) we observe that the temperature $\theta(\eta)$ and concentration profiles $\phi(\eta)$ decrease with increasing ion-slip parameter β_i.

Figures (5.14)-(5.16) show the influence of permeability parameter k^* on the velocity components $f'(\eta)$, $f(\eta)$ and $g(\eta)$. As shown in these figures, all the velocity components are increasing with increasing values of the permeability parameter k^*. It is expected that, increase in the permeability of porous medium lead

to a rise in the flow of the fluid through it since when the holes of the porous medium become large, the resistance of the medium may be neglected.

Figures (5.17) and (5.18) represent the influence of Schmidt number Sc and Soret number Sr on concentration profiles $\phi(\eta)$ repectively. It can be observed from these figures that the concentration decreases with increasing Schmidt number and increases with increasing Soret number.

Figures (5.19)-(5.23) represent velocity components $f'(\eta)$, $f(\eta)$ and $g(\eta)$, temperature $\theta(\eta)$ and concentration $\phi(\eta)$ for various values of Suction/Blowing parameter S. Here, $S > 0$ shows the suction and $S < 0$ shows the blowing. The axial and cross-flow velocities decrease with increasing S, whereas the transverse velocity $f(\eta)$ increases with increasing S. The temperature and species concentration decrease as the parameter S increases.

Figure (5.24) represents skin-friction coefficient $f''(0)$ as a function of Hall current parameter β_e for various values of ion-slip parameter β_i .Viscous stress acting on the surface of the plate is estimated using the skin-friction coefficient. It is clear that skin-friction increases with increasing ion-slip β_i and Hall current β_e .

Figure (5.25) shows the shear stress $g'(0)$ in z-direction against Hall current parameter β_e for various values of ion-slip parameter β_i . Shear stress in z-direction $g'(0)$ increases with increasing values of β_e when $\beta_e \leq 1$, but decreases with increasing values of Hall current parameter β_e greater than unity. Shear stress in z-direction $g'(0)$ increases with increasing value of ion-slip β_i.

Figures (5.26) and (5.27) show that rate of heat and mass transfer decrease with increase in ion slip β_i. Due to increase in ion slip, the rate of heat transfer increases and the rate of mass transfer decreases.

5.5. Conclusion

The steady free-convective laminar flow of an incompressible viscous and electrically conducting fluid with heat and mass transfer over a porous flat plate in the presence of transverse magnetic field, Hall and ion-slip currents embedded in porous medium has been investigated. The non-linear governing equations together with the boundary conditions are reduced to a system of non-linear ordinary differential equations using the similarity transformations. The system of non-linear ordinary differential equations are solved by shooting procedure using fourth order Runge-Kutta Method.

From the present study, we can conclude that all the instantaneous flow characteristics are affected by the ion-slip parameter β_i. The velocity profiles $f'(\eta), f(\eta)$ increase with increasing ion-slip parameter β_i. The velocity distribution i.e., cross flow velocity $g(\eta)$ decreases with increasing values of β_i. Results are presented graphically to illustrate the variation of shear stress, Nusselt number and Sherwood number with various parameters.

In this study the following conclusions are brought out:

- Skin-friction increases with increasing ion-slip β_i and Hall current β_e.
- Shear stress in z-direction $g'(0)$ increases with increasing values of β_e when $\beta_e \leq 1$, but decreases with increasing values of Hall current parameter β_e greater than unity.
- The rate of heat transfer $\theta'(0)$ decreases, with increase of ion-slip β_i and Hall current β_e .
- The rate of mass transfer $\phi'(0)$ decreases with increase of ion-slip β_i and increases with increase of Hall current β_e.

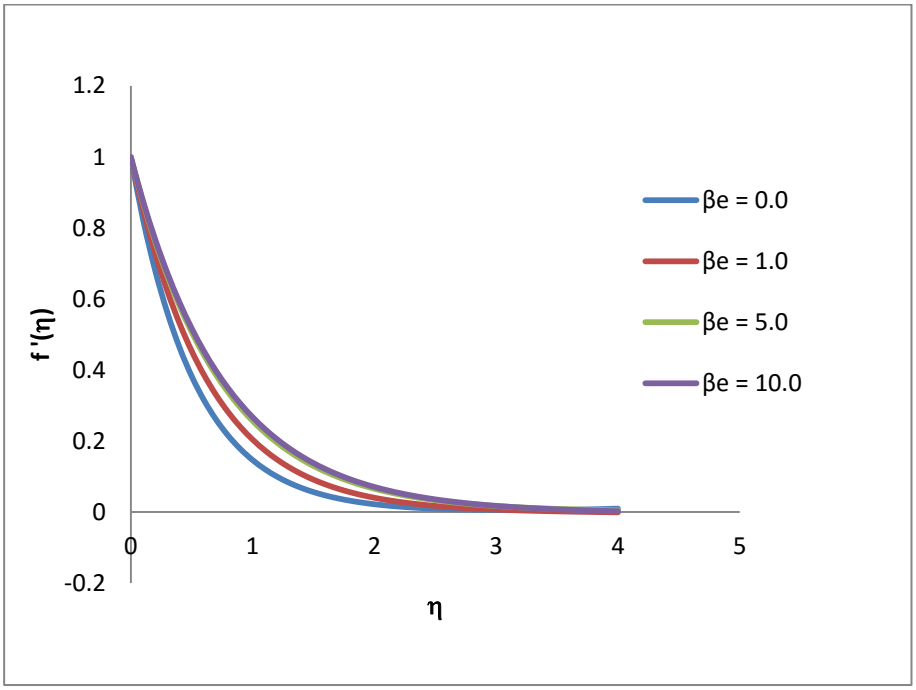

Fig 5.2 Axial velocity of $f'(\eta)$ for various values of Hall current parameter β_e; Pr=7.0; Sc=0.3; Sr=0.3; k=2.0; Re=1.0; S=0.1; M=2.0; βi=1.0*

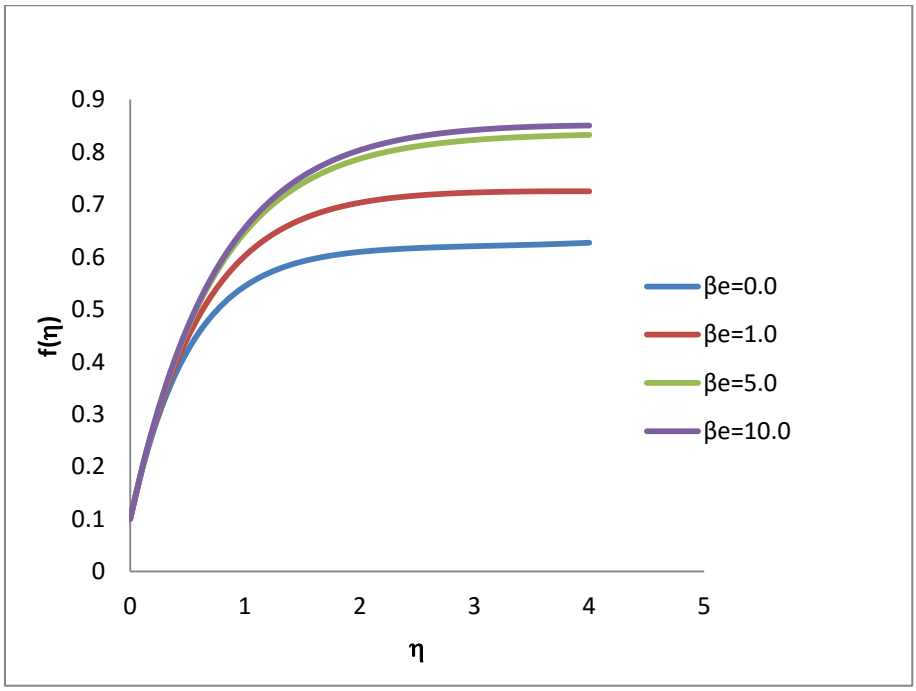

Fig 5.3 Transverse velocity of $f(\eta)$ for various values of Hall current β_e; Pr=7.0; Sc=0.3;Sr=0.3; k=2.0; Re=1.0; S=0.1; M=2.0; βi=1.0*

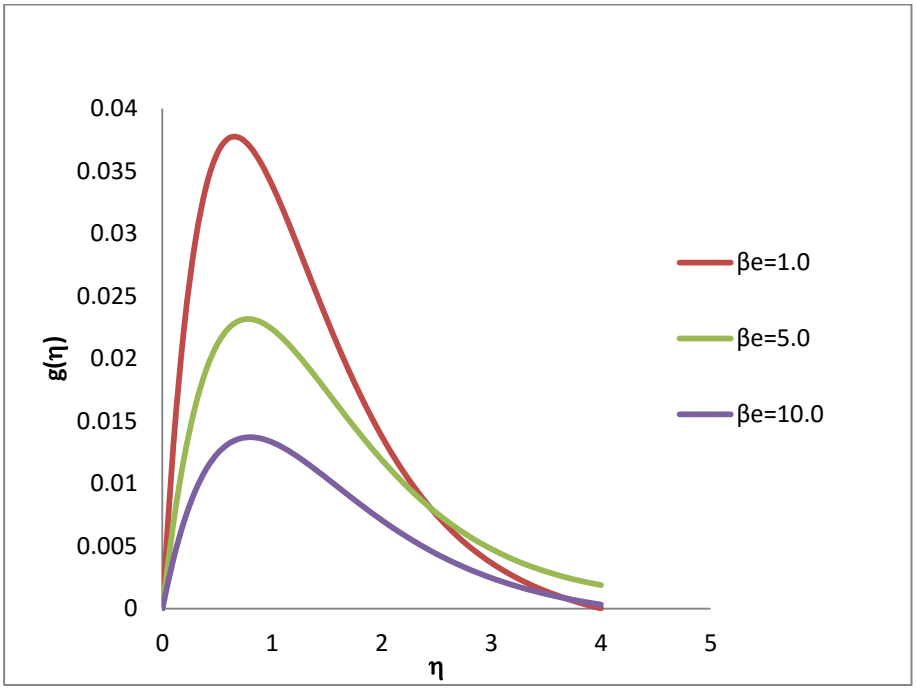

Fig 5.4 Cross flow velocity of $g(\eta)$ for various values of Hall current parameter β_e; Pr=7.0; Sc=0.3; Sr=0.3; k=2.0; Re=1.0; S=0.1; M=2.0; βi=1.0*

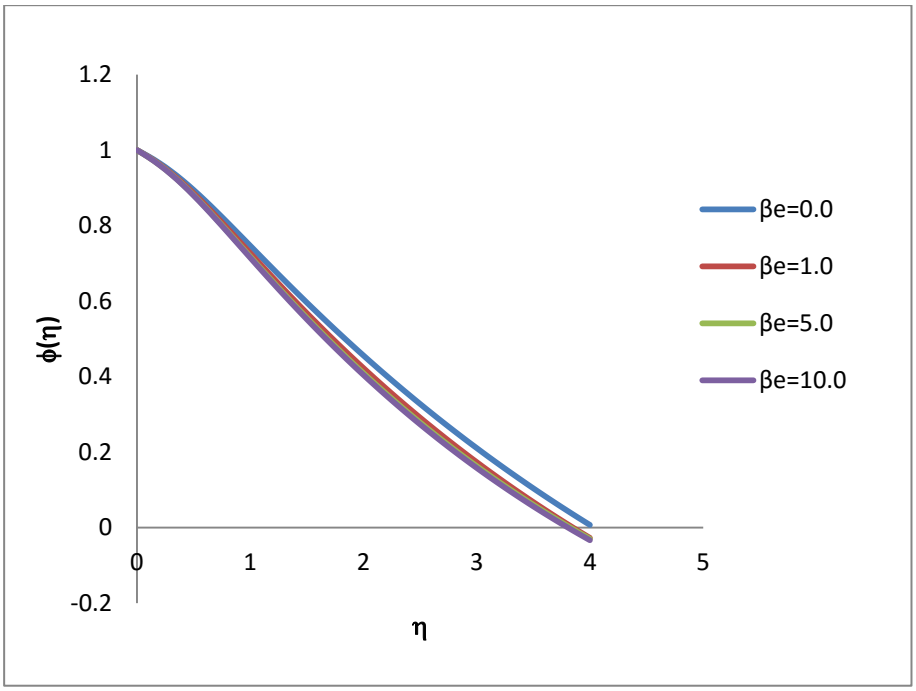

Fig 5.5 Concentration profiles $\phi(\eta)$ for various values of Hall current β_e; Pr=7.0; Sc=0.3; Sr=0.3; k=2.0; Re=1.0; S=0.1; M=2.0; βi=1.0*

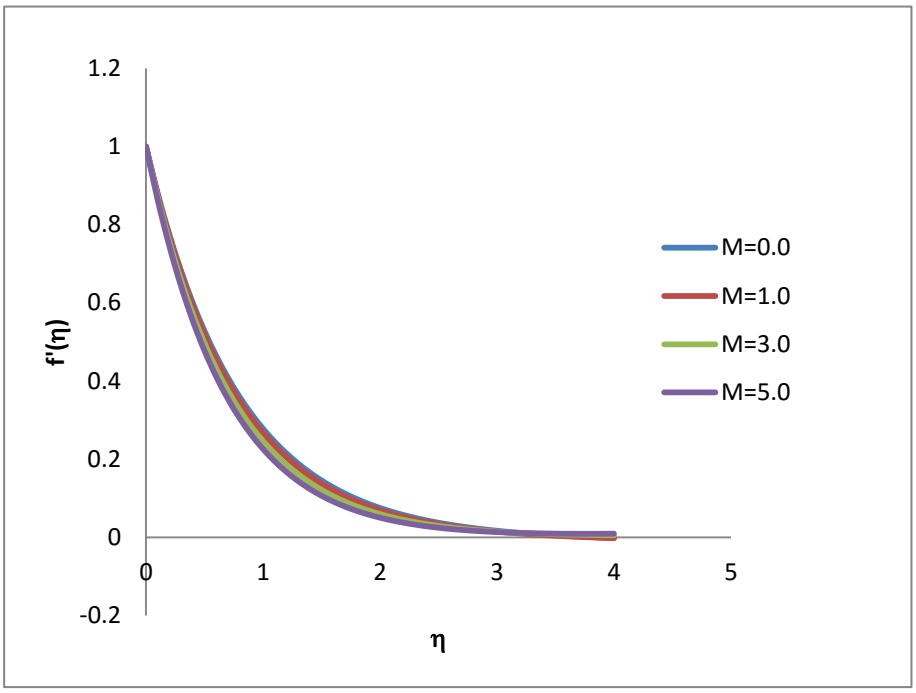

Fig 5.6 Axial velocity of $f'(\eta)$ for various values of magnetic parameter M; Pr=7.0; Sr=0.3; Sc=0.3; S=0.1; k=2.0; Re=1.0; β_i=1.0; β_e=5.0*

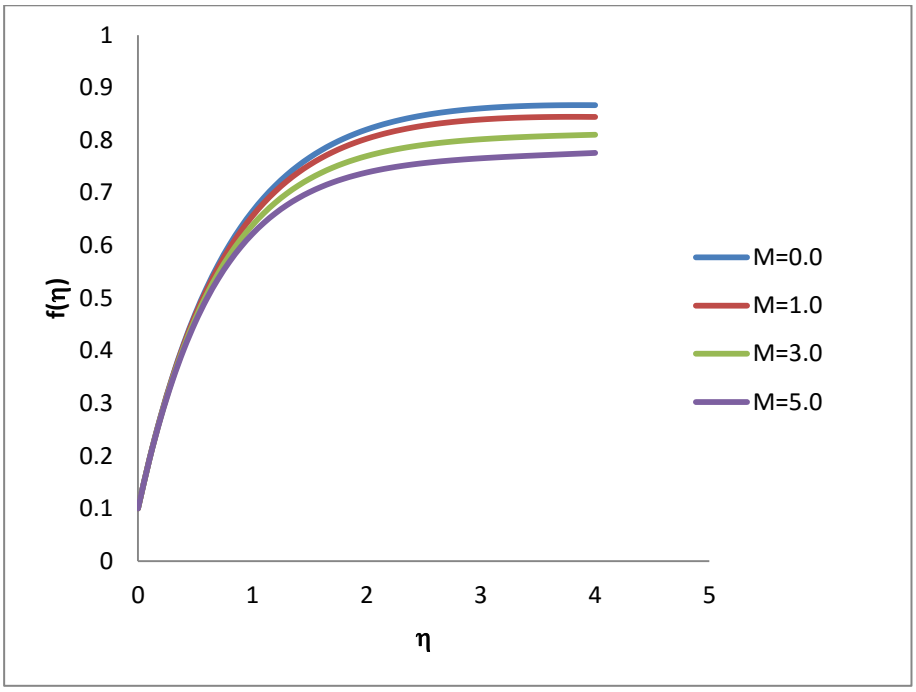

Fig 5.7 Transverse velocity of $f(\eta)$ for various values of magnetic parameter M; Pr=7.0; Sr=0.3; Sc=0.3; S=0.1; k=2.0; Re=1.0; β_i=1.0; β_e=5.0*

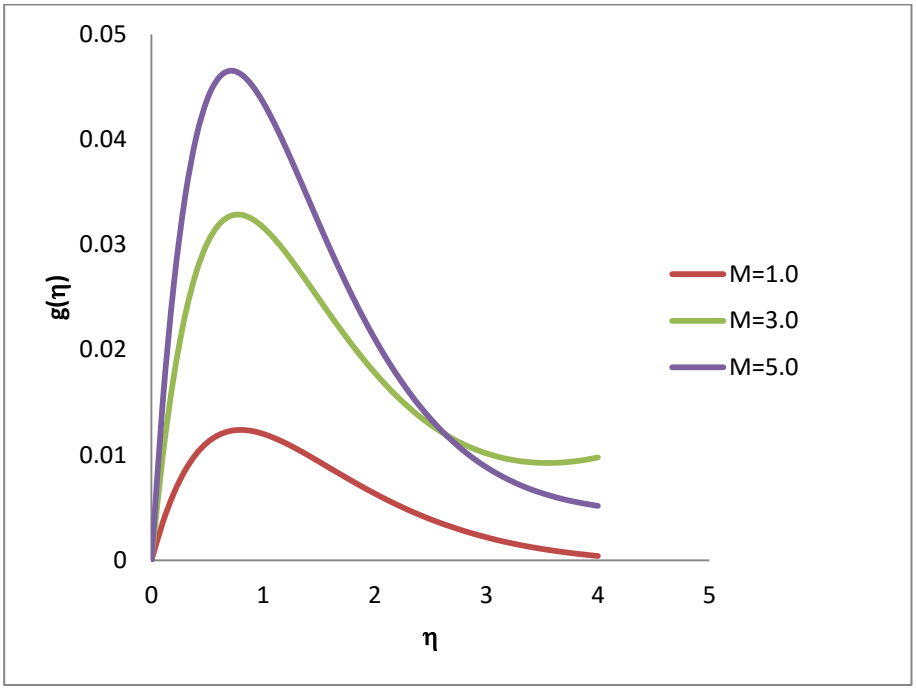

Fig 5.8 Cross flow velocity of $g(\eta)$ for various values of magnetic parameter M; Pr=7.0; Sr=0.3; Sc=0.3; S=0.1; k=2.0; Re=1.0; β_i=1.0; β_e=5.0*

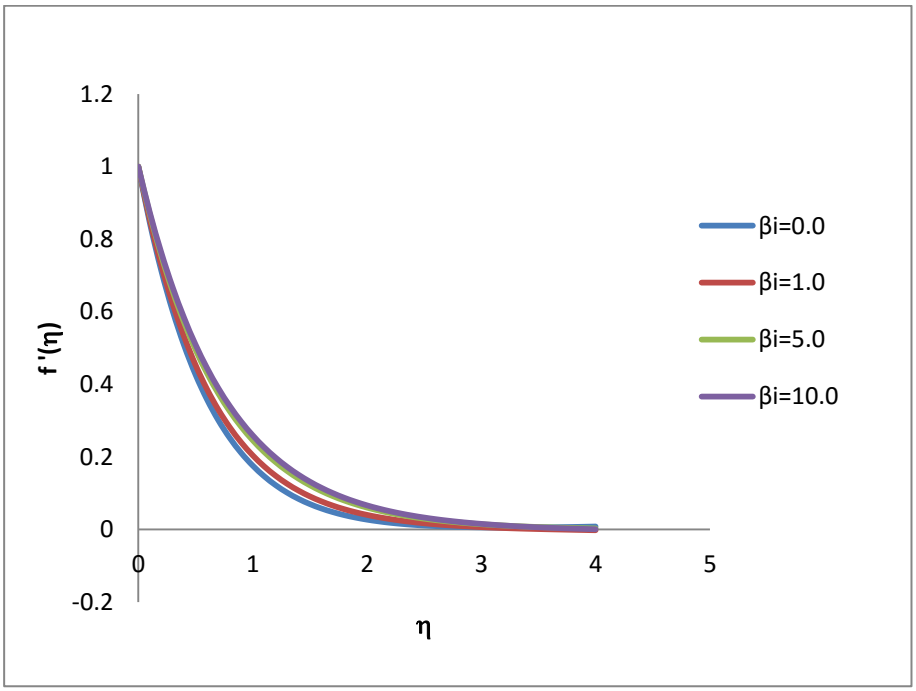

Fig 5.9 Axial velocity of $f'(\eta)$ for various values of ion-slip parameter β_i; Pr=7.0; Sc=0.3; Sr=0.3; k=2.0; Re=1.0; S=0.1; M=2.0; β_e=1.0*

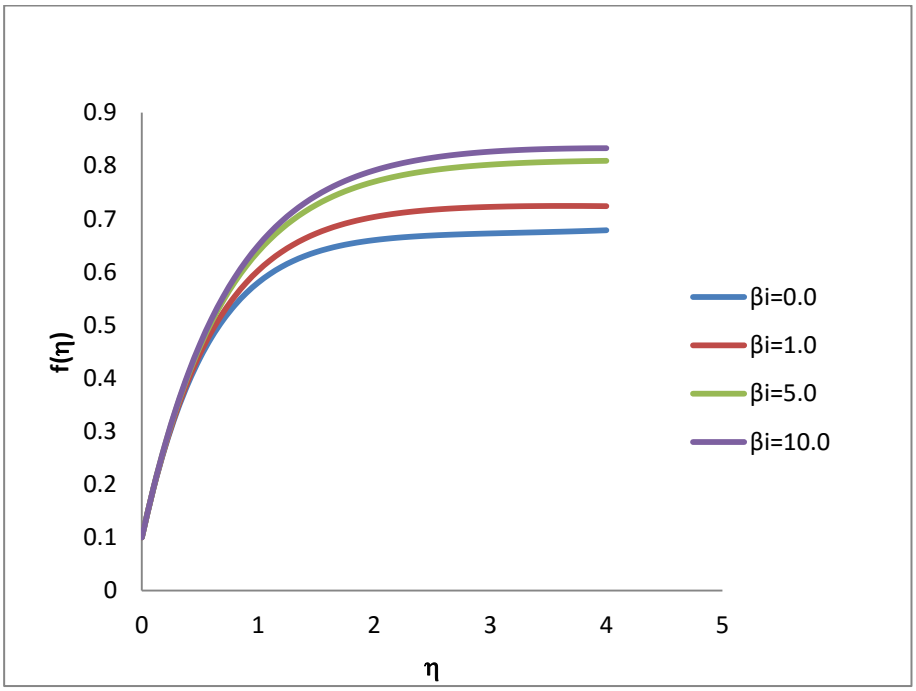

Fig 5.10 Transverse velocity of $f(\eta)$ for various values of ion-slip parameter β_i; Pr=7.0; Sc=0.3; Sr=0.3; k=2.0; Re=1.0; S=0.1; M=2.0; β_e=1.0*

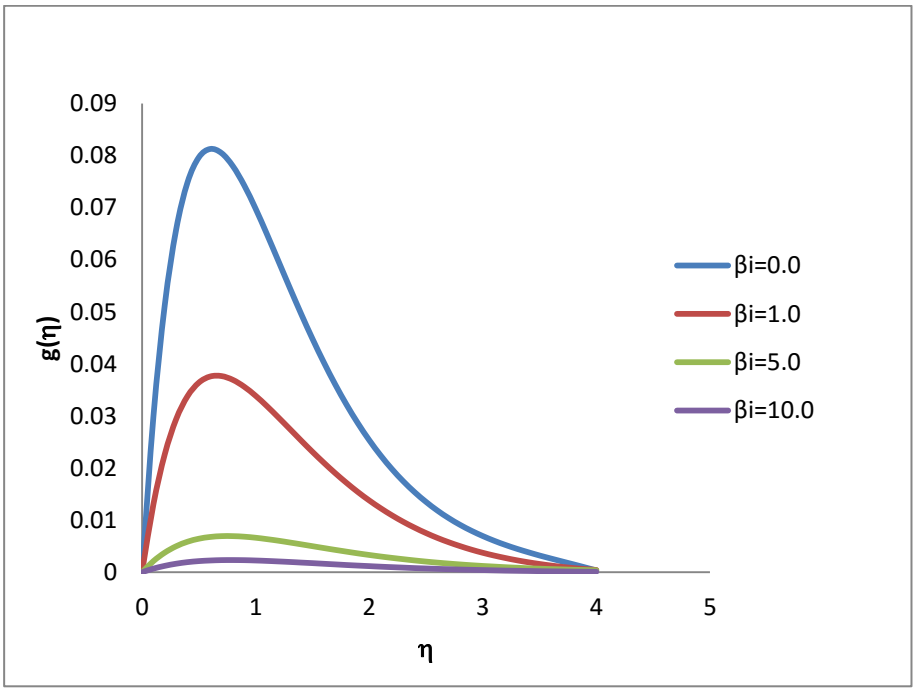

Fig 5.11 Cross flow velocity of $g(\eta)$ for various values of ion-slip parameter β_i; Pr=7.0; Sc=0.3; Sr=0.3; k=2.0; Re=1.0; S=0.1; M=2.0; β_e=1.0*

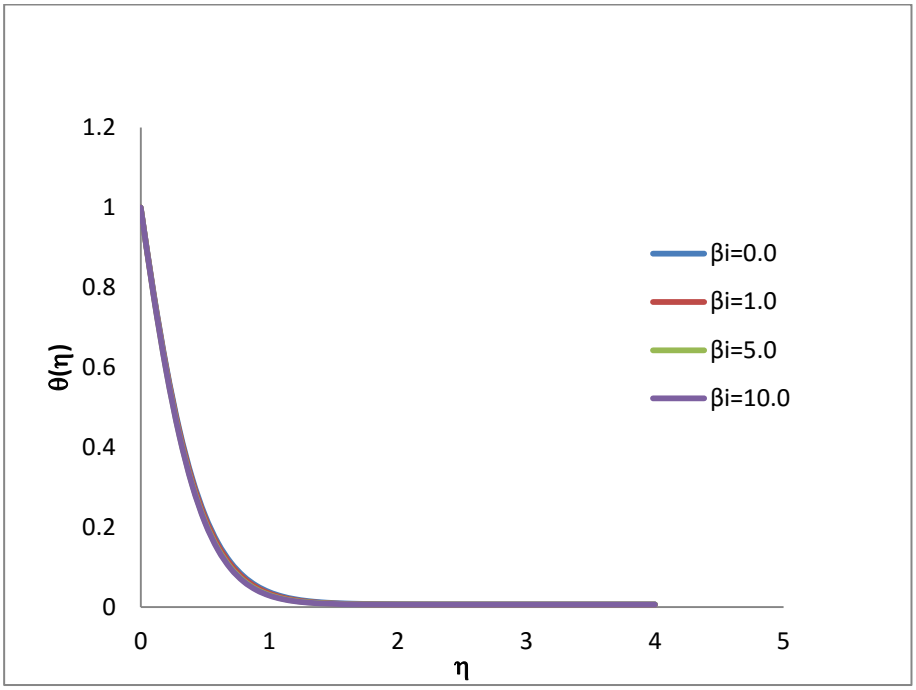

Fig 5.12 Temperature profiles of $\theta(\eta)$ for various values of ion-slip parameter β_i; Pr=7.0; Sc=0.3; Sr=0.3; k=2.0; Re=1.0; S=0.1; M=2.0; β_e=1.0*

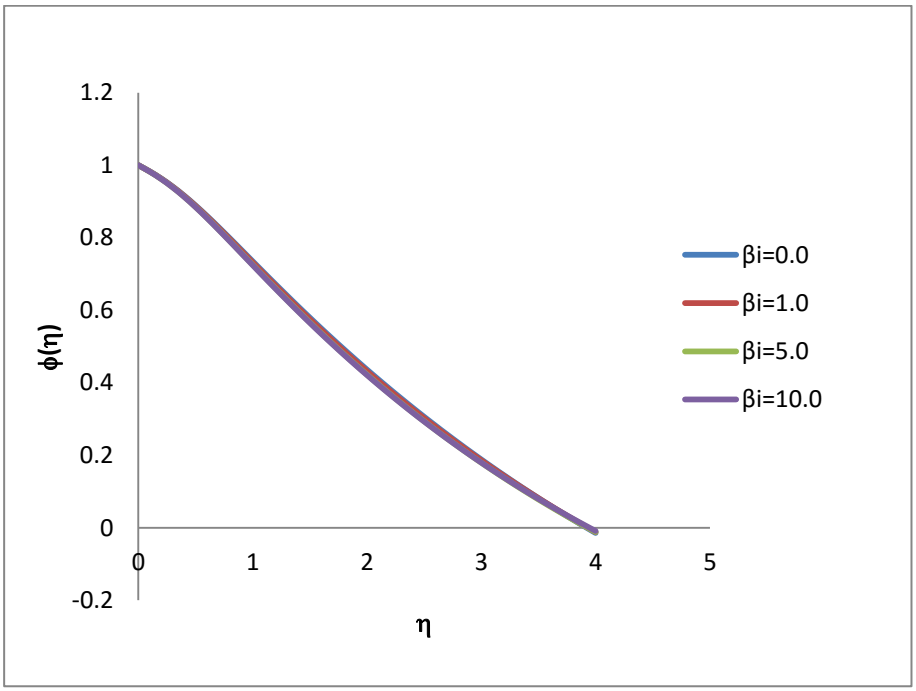

Fig 5.13 Concentration profiles $\phi(\eta)$ for various values of ion-slip parameter β_i; Pr=7.0; Sc=0.3; Sr=0.3; k=2.0; Re=1.0; S=0.1; M=2.0; β_e=1.0*

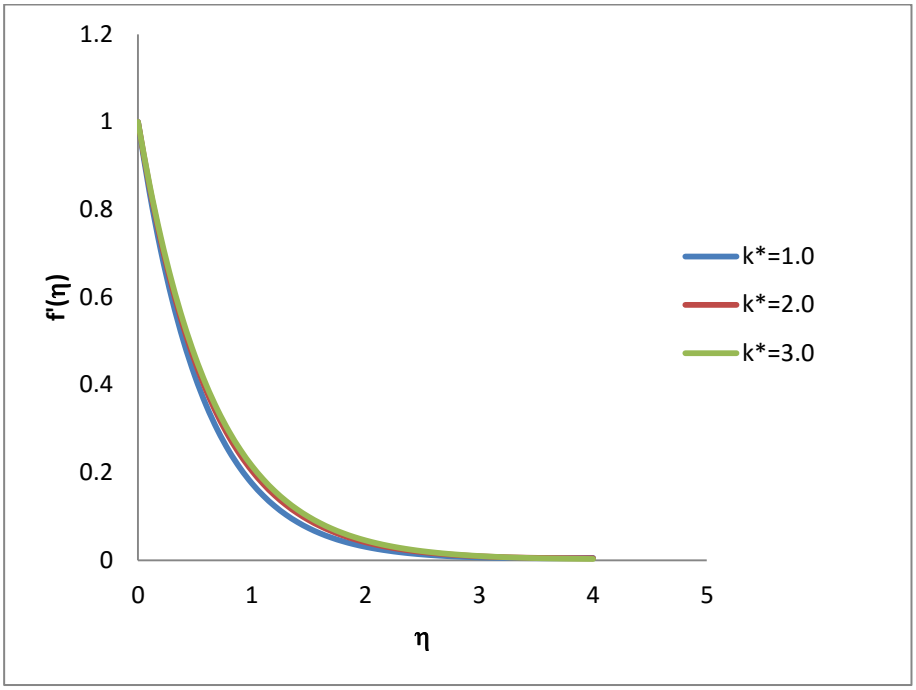

Fig 5.14 Axial velocity of $f'(\eta)$ for various values of permeability parameter k^*; Pr=7.0; Sr=0.3; Sc=0.3; S=0.1; Re=1.0; β_i=1.0; β_e=1.0

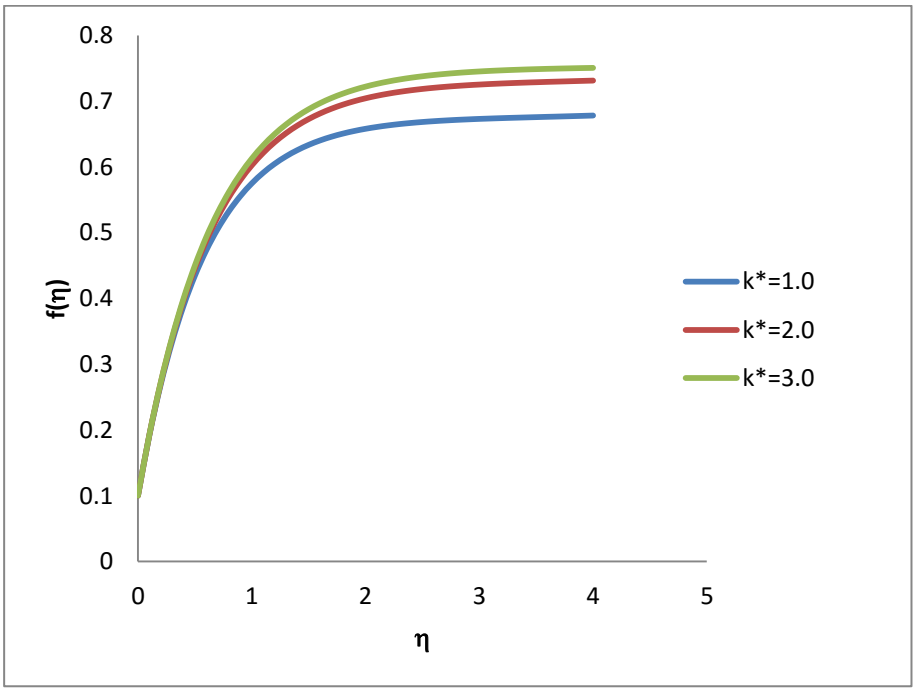

Fig 5.15 Transverse velocity of $f(\eta)$ for various values of permeability parameter k^*; Pr=7.0; Sr=0.3; Sc=0.3; S=0.1; Re=1.0; β_i=1.0; β_e=1.0

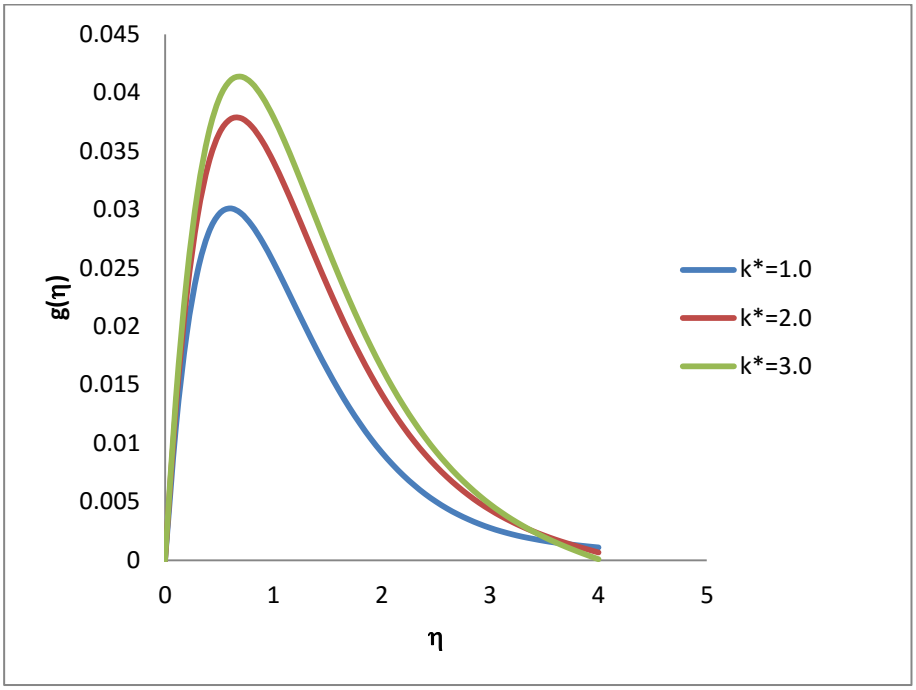

Fig 5.16 Cross flow velocity of $g(\eta)$ for various values of permeability parameter k^*;Pr=7.0; Sr=0.3; Sc=0.3; S=0.1; Re=1.0; β_i=1.0; β_e=1.0

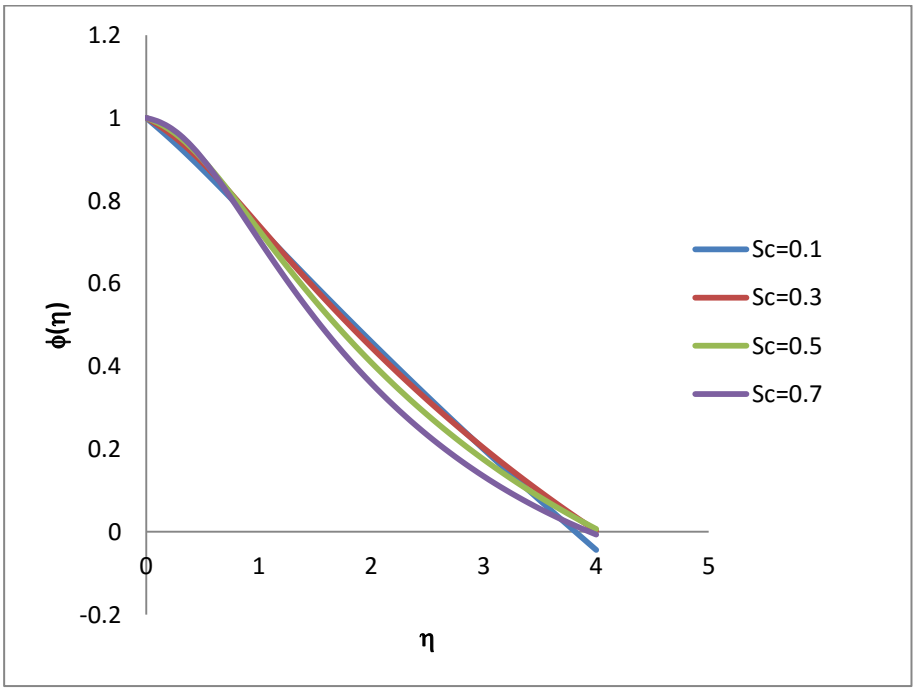

Fig 5.17 Concentration profiles $\phi(\eta)$ for various values of Schmidt number Sc; Pr=7.0; Sr=0.3; S=0.1; Re=1.0; k=1.0; β_i=1.0; β_e=1.0*

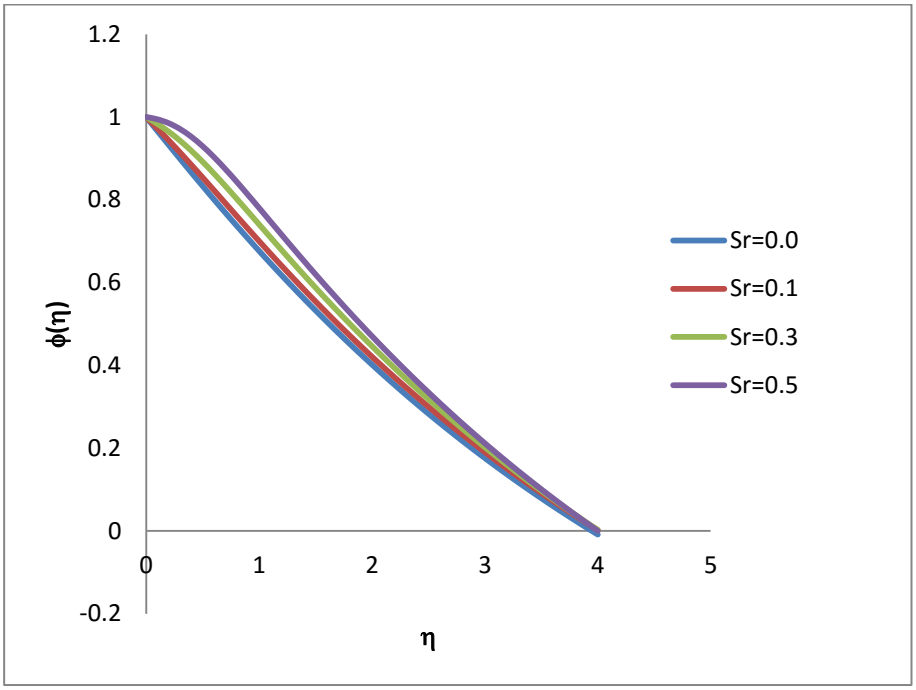

Fig 5.18 Concentration profiles $\phi(\eta)$ for various values of Soret number Sr; Pr=7.0; Sr=0.3; S=0.1; Re=1.0; k=1.0; β_i=1.0; β_e=1.0*

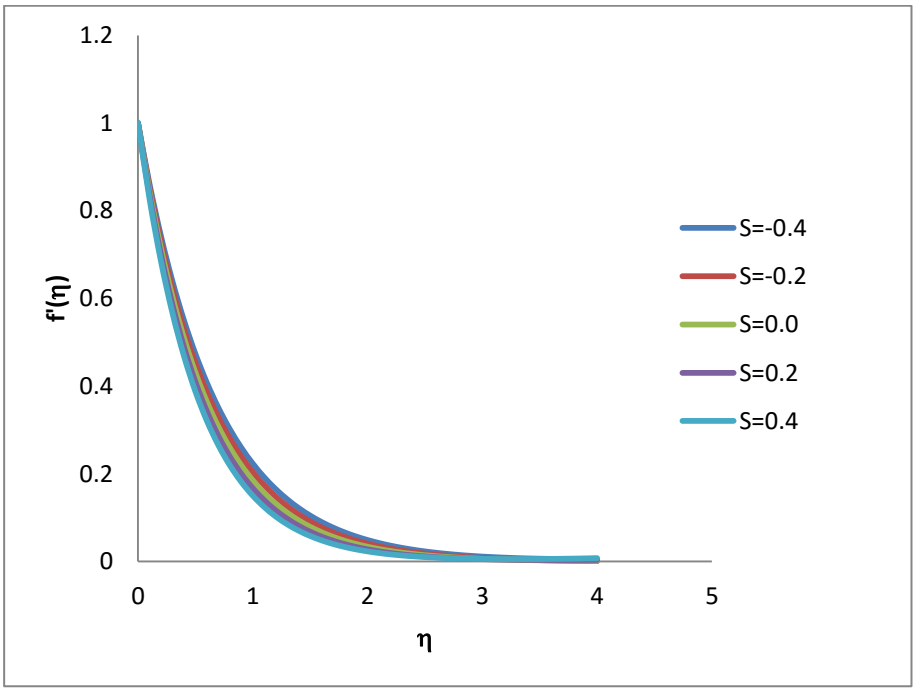

Fig 5.19 Axial velocity of $f'(\eta)$ for various values of Suction/Blowing parameter S; Pr=7.0; Sr=0.3; Sc=0.3; Re=1.0; k=1.0; β_i=1.0; β_e=1.0; M=2.0*

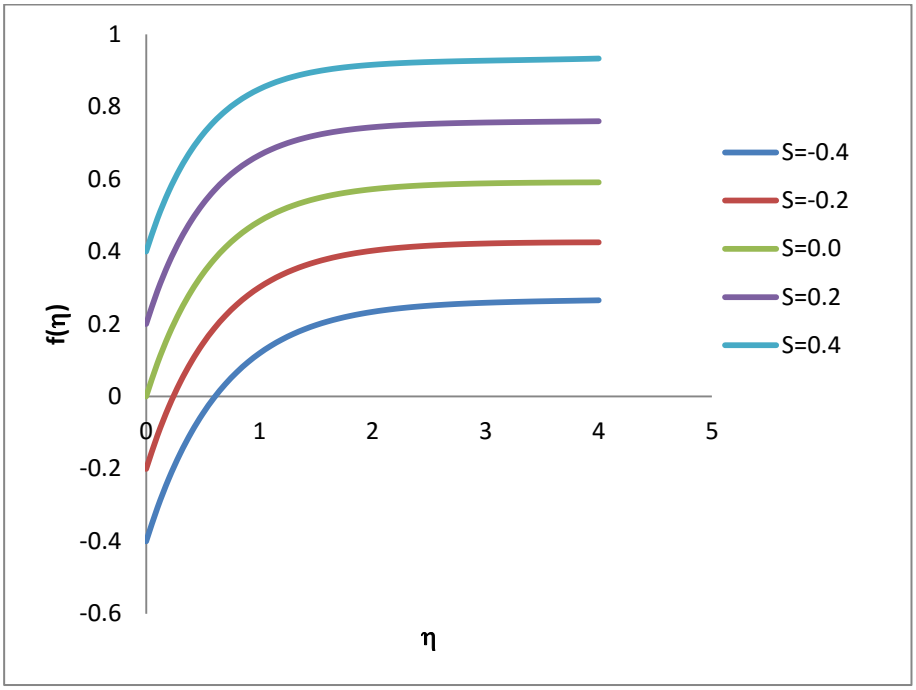

Fig 5.20 Transverse velocity of $f(\eta)$ for various values of Suction/Blowing parameter S; Pr=7.0; Sr=0.3; Sc=0.3; Re=1.0; k=1.0; β_i=1.0; β_e=1.0; M=2.0*

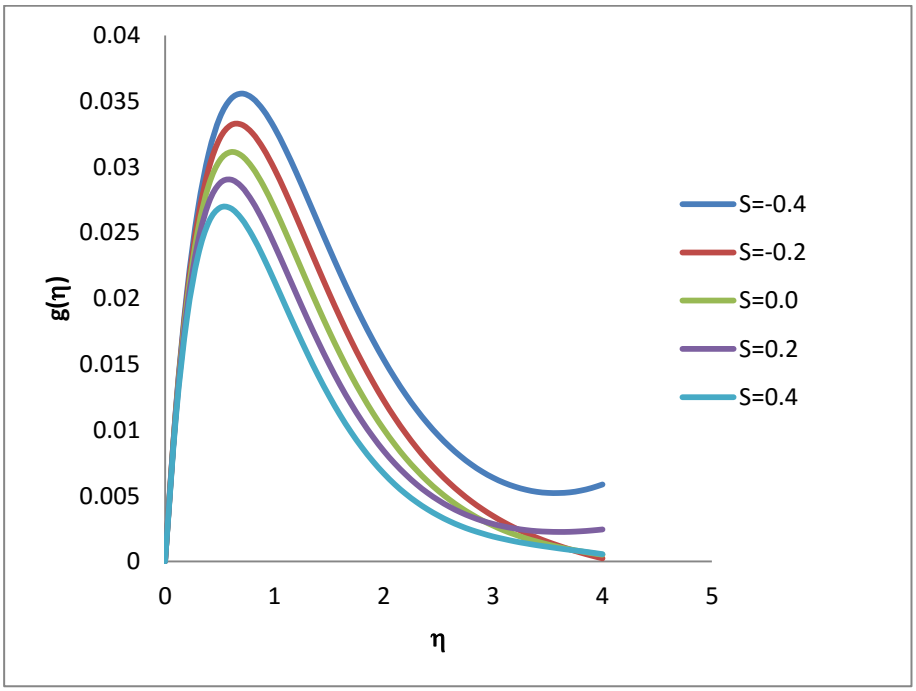

Fig 5.21 Cross flow velocity of $g(\eta)$ for various values of Suction/Blowing parameter S; Pr=7.0; Sr=0.3; Sc=0.3; Re=1.0; k=1.0; β_i=1.0; β_e=1.0; M=2.0*

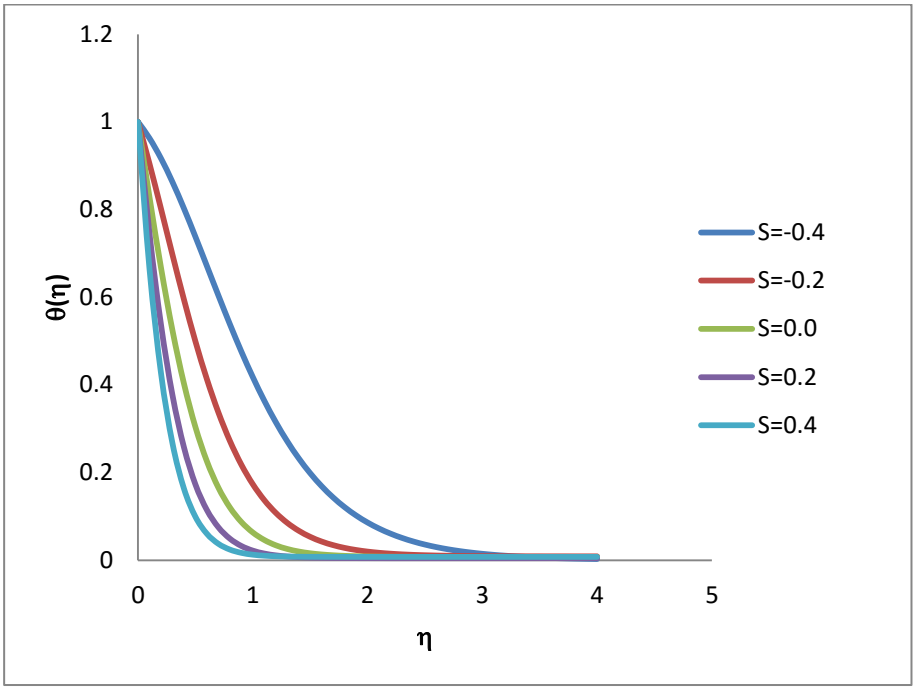

Fig 5.22 Temperature profiles of $\theta(\eta)$ for various values of Suction/Blowing parameter S; Pr=7.0; Sr=0.3; Sc=0.3; Re=1.0; k=1.0; β_i=1.0; β_e=1.0; M=2.0*

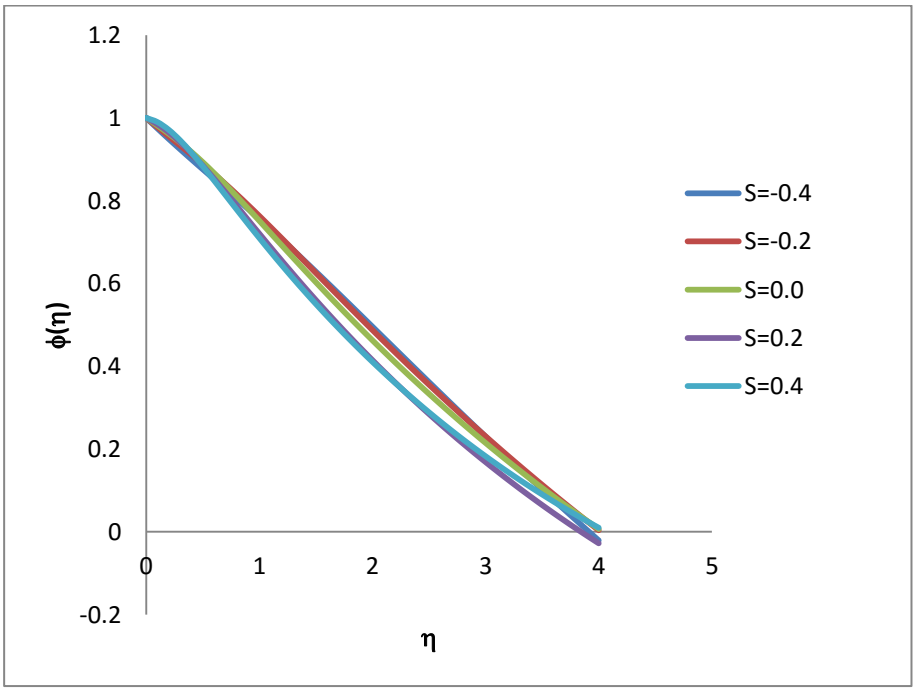

Fig 5.23 Concentration profiles $\phi(\eta)$ for various values of Suction/Blowing parameter S; Pr=7.0; Sr=0.3; Sc=0.3; Re=1.0; k=1.0; β_i=1.0; β_e=1.0; M=2.0*

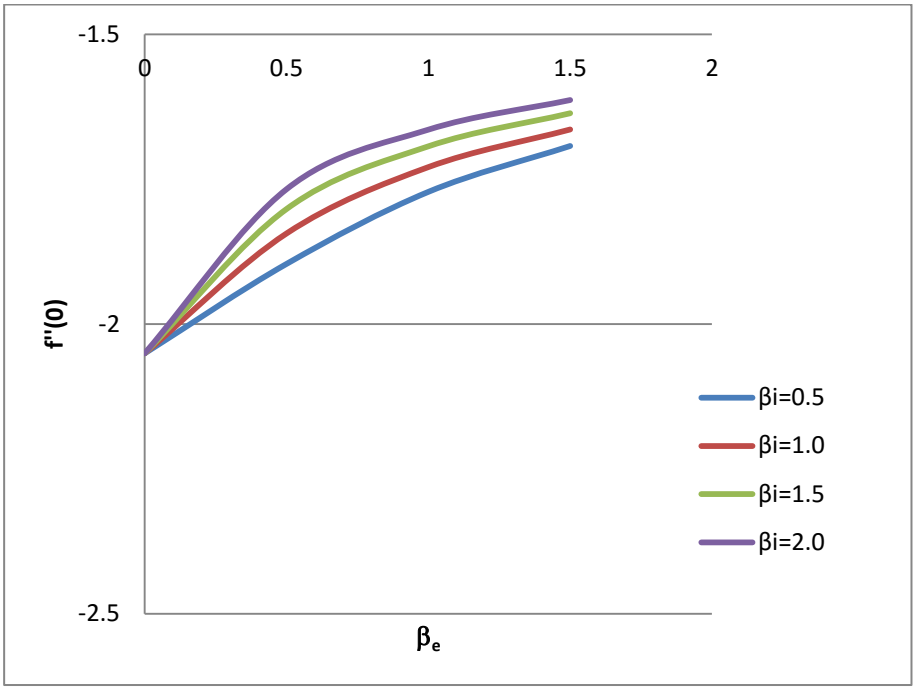

Fig 5.24 Skin-friction coefficient $f''(0)$ against Hall current parameter β_e for various values of ion-slip parameter β_i; Pr=7.0; Sc=0.3; Sr=0.3; k=1.0; Re=1.0; S=0.1; M=2.0*

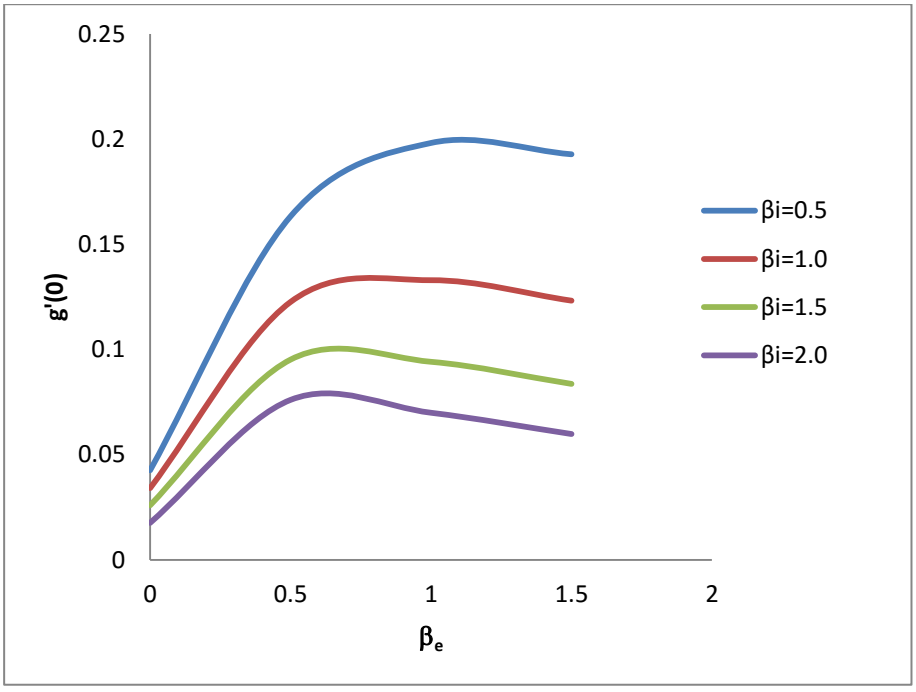

Fig 5.25 Shear stress in z-direction $g'(0)$ against Hall current parameter β_e for various values of ion-slip parameter β_i ; Pr=7.0; Sc=0.3; Sr=0.3; k=1.0; Re=1.0; S=0.1; M=2.0*

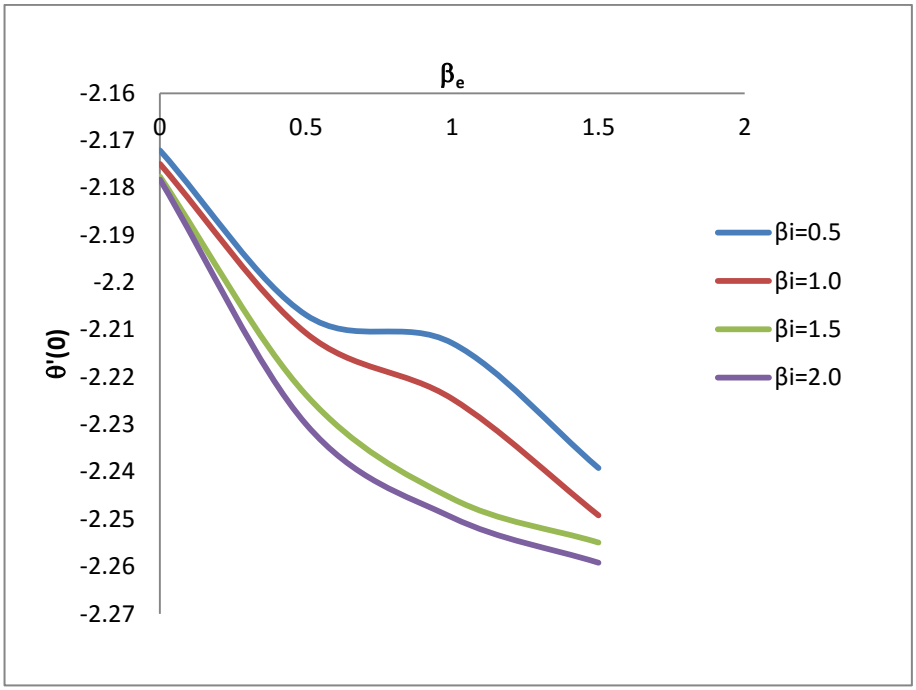

Fig 5.26 Temperature gradient at the plate $\theta'(0)$ against Hall current parameter β_e for various values of ion-slip parameter β_i ; Pr=7.0; Sc=0.3; Sr=0.3; k=1.0; Re=1.0; S=0.1; M=2.0*

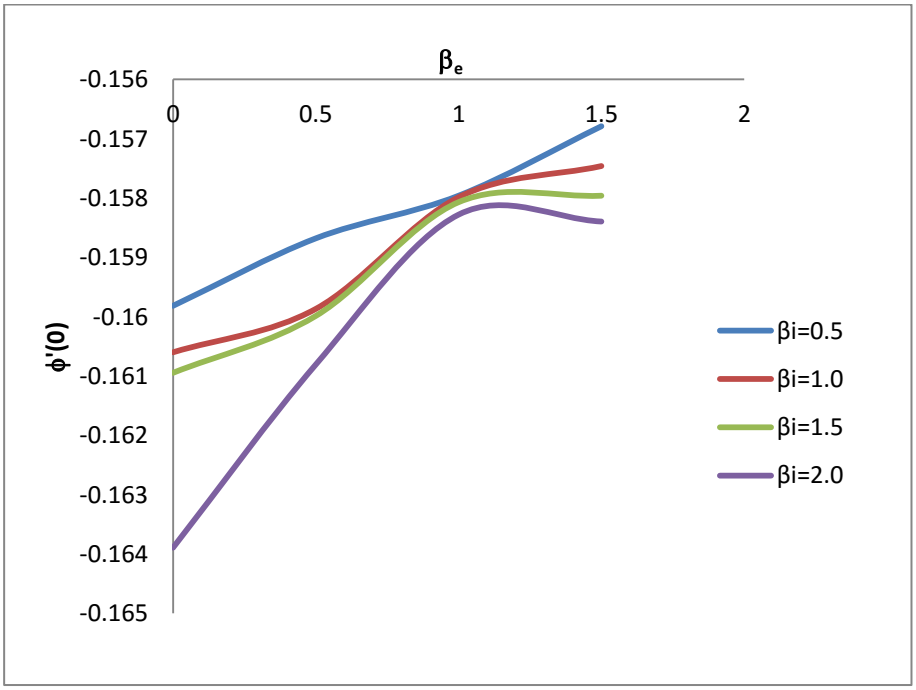

Fig 5.27 Concentration gradient at the plate $\phi'(0)$ against Hall current parameter β_e for various values of ion-slip parameter β_i; Pr=7.0; Sc=0.3; Sr=0.3; k=1.0; Re=1.0; S=0.1; M=2.0*